Electronic Supplementary Material (ESI) for Journal of Materials Chemistry A.

Operando Probing of Li-insertion on $LiMn_2O_4$ Cathodes by Spectroscopic Ellipsometry

A. Morata[1,], V. Siller[1], F.Chiabrera[1], M. Nuñez[1], R. Trocoli[1], M. Stchakovsky[2], A. Tarancon[1,3,*]*

[1]IREC, Jardins de les Dones de Negre 1, Planta 2, 08930, Sant Adrià del Besòs, Spain
[2]HORIBA Scientific, Avenue de la Vauve, Passage Jobin Yvon, 91120 Palaiseau, France
[3]ICREA, Passeig Lluís Companys 23, 08010, Barcelona, Spain

1. Structural analysis

Supplementary Figure 1 shows X-ray diffractograms obtained from the PLD deposited $LiMn_2O_4$ film. A measurement on the substrate is included as reference in the same plot for comparison. A peak at 2Θ=18° evidences the existence of $LiMn_2O_4$ spinel phase with a preferential orientation in the (111) plane. The higher intensity of this peak evidences a clear preferential orientation, as discussed elsewhere. These results are consistent with the one obtained with the same PLD multilayering procedure and discussed in previous publications[1].

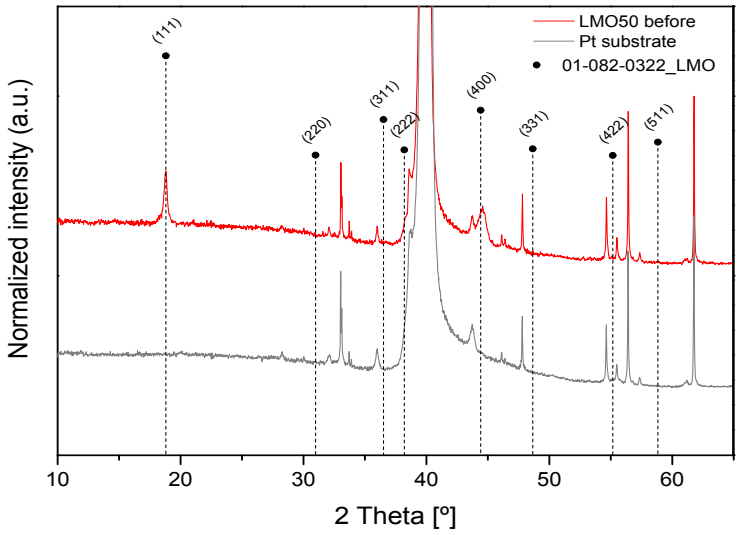

Supplementary Figure 1. XRD of the $LiMn_2O_4$ thin film deposited by PLD (red line). The diffractogram from the pristine substrate is also presented for comparison (grey line).

2. Construction of the ellipsometric model for the $LiMn_2O_4$ layer

In order to attain a comprehension of the results obtained from ellipsometry, the acquired data points are compared with those arisen from a previously generated model. The quality of the model and the data (range and number of wavelengths screened in each measurement) are key

for attaining physically meaningful results. In this section we describe step by step the procedure followed for the model construction.

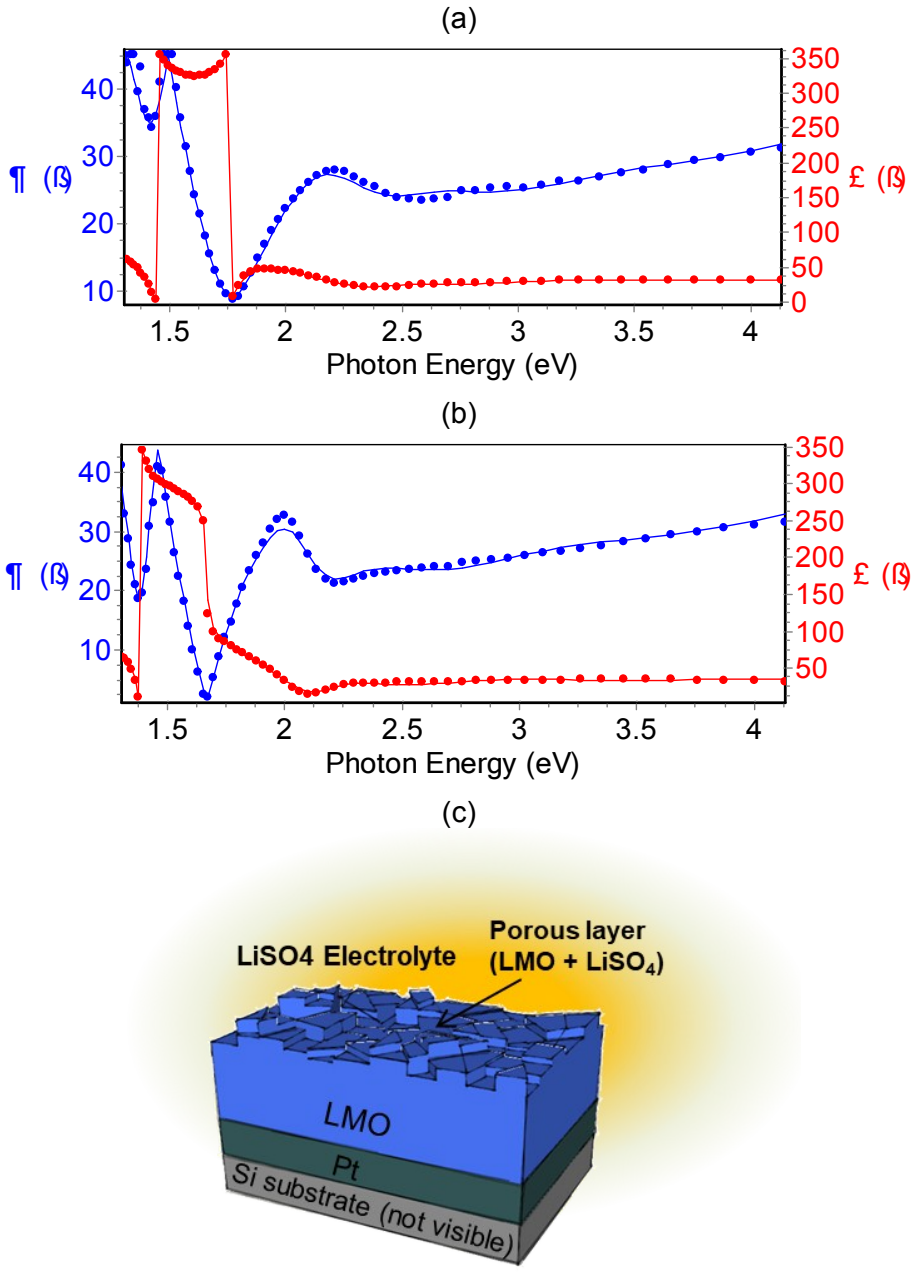

Supplementary Figure 2. Results obtained from the SE measurement in a sample maintained at 0.350 and 1.050V (a) and (b), respectively. The lines represent the fitting of the generated model. (c) graphical representation of the model used for the fitting.

The first step is to define a reasonable function that can describe the optical properties of the material under test. Here we have used Tauc-Lorentz formulation to parametrize ε_r, ε_i as a function of photon energy[1]. The expression of this formula is:

$$\varepsilon_i = \begin{cases} \sum_{j=1}^{N} \frac{1}{E} \frac{A_j E_j C_j (E - E_g)^2}{(E^2 - E_j^2)^2 + C_j^2 E^2} & for\ E > E_g \\ 0 & for\ E \leq E_g \end{cases}$$

Where E is the photon energy, E_g is the optical band gap, E_j , A_j and C_j are the central energy, the amplitude and the broadening term of the j oscillator, respectively. The real part of the dielectric function (ε_r) is obtained from the expression of ε_i by means of the Kramers-Kroning integration.

We can make use of previous bibliography giving information about the band configuration and light absorption on spinel MnO_2 and $LiMn_2O_4$[2,3]. A low energy absorption is expected both in MnO_2 (2.3 eV) and $LiMn_2O_4$ (1.9eV), attributed to O^{2-}(2p) to Mn^{4+} or Mn^{3+} (t_{2g}) transitions. These absorption bands will be represented by a single oscillator, which amplitude and resonant peak energy are led free in the fitting[4]. Also, two higher energy absorption bands are anticipated at 2.8-3 eV and 3.4-3.6 eV, corresponding to the electronic transition from O^{2-}(2p) to Mn^{4+}(e_g) and Mn^{3+}(e_g), respectively. Every one of these two last bands will be represented by a specific Lorentz oscillator, as they are expected to evolve differently with Li content variation. Finally, a fourth oscillator is used in order to achieve a reasonable fitting at higher energies, accounting with the transitions in the limit and above the measurement range. This last component will be fixed as common to both fully oxidized and fully reduced sample states. As the aim is to obtain a common model for all the range *x*, representing the Li content in $Li_xMn_2O_4$, the selected parameters describing every one of the oscillators must be capable to provide a reasonable fitting for all x. *Supplementary Figure 2a* shows the SE measurements obtained in the electrochemical chamber at the maximum and minimum values of *x* (i.e. 0.350 and 1.050 V, respectively). In the sake of simplicity, it is our aim to minimize the number of fitting variables, so we fix several parameters as common to both states: the fourth oscillator parameters and the broadening terms of all the oscillators. The optical properties of the electrolyte are also introduced as ambient material. are also included in the model. The procedure is the following: (i) A general model is constructed based on the previous considerations, with a main layer thickness, a porous surface layer that accounts the layer roughness and porosity and a four oscillators Tauc-Lorentz function representing the optical properties of the $Li_xMn_2O_4$ material. The Sketch in *Supplementary Figure 2b* is a graphical representation of the model. (ii)A first fitting of that model is carried out using the SE measurements obtained in the higher and lower values of *x*. For this, the two set of data (obtained at 0.350 and 1.050V) are simultaneously fit in order to fix an average value for the variables that will be considered common. (iii) The as-obtained values are separately fit in both extremes of *x* (i.e. 0.350 and 1.050V), fixing the common values and releasing all the rest.
The fitting of the as-generated model is presented as a red line in *Supplementary Figure 2a*. *Table 1* summarizes the values for all the parameter at 0.35 and 1.05 V, in which the common values have been remarked using italics.

Table 1. Parameters of the model arising from the fitting at two different potentials (0.350 and 1.050V). The magnitudes fixed as common for both potentials are marked in italics.

Parameter	units	Fit at 0.350 V	Fit at 1.050 V
L1 Thickness	nm	261±5	269±6
L2 Thickness	nm	51±1	51±1
L2 %		61±1	59±1
Eg	eV	0.6±0.1	0.8±0.1

ε_∞	eV	2.8±0.1	2.6±0.1
A1		0.7±0.2	0.7±0.2
E1	eV	1.57±0.05	1.54±0.03
C1	*eV*	*0.7± 0.5*	*0.7±0.5*
A2		0.5±0.2	9±1
E2	eV	1.9±0.2	2.82±0.05
C2	*eV*	*1± 1*	*1±1*
A3		9±1	4±1
E3	eV	3.17±0.05	3.5±0.2
C3	*eV*	*2±1*	*2±1*
A4		*3±2*	*3±2*
E4	*eV*	*4±1*	*4±1*
C4	*eV*	*1±1*	*1±1*

3. Fast acquisition procedure

A procedure has been followed that allows to overcome the time limitation imposed by the monochromator in the spectroscopic ellipsometry measurement. It consists on the measurement of the ellipsometric variables (i.e. ψ and Δ) at a single wavelength while imposing the desired voltage cycle to the sample. In this proof of concept, a potential step was introduced with the aim of demonstrating the time resolution capabilities of the technique. This procedure is repeated at different fixed photon energies in the desired range. In this case we restrict to the window allowed by the $LiSO_4$ electrolyte absorption, which goes from 1.47 to 4.13 eV. 19 different energies were selected in this range in order to construct a whole spectroscopic ellipsometry dataset. ***Supplementary Figure 3*** shows an example of a single measurement at 1.968eV. The high sensitivity of the technique is evidenced.

(a)

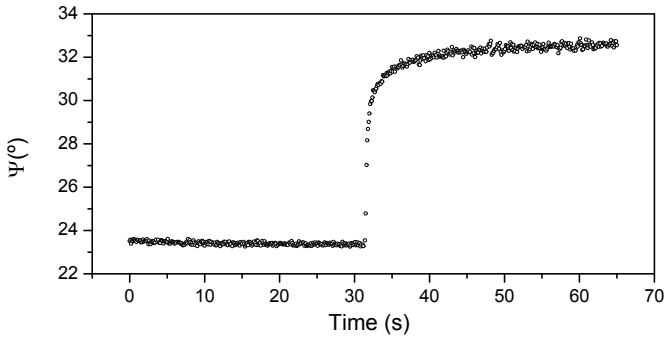

(b)

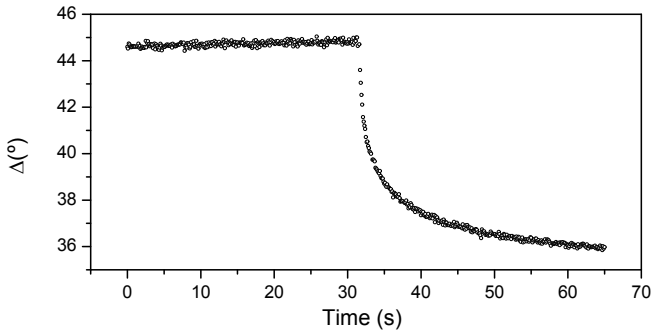

Supplementary Figure 3. Outputs from an ellipsometry measurement at a photon energy 1.968eV (630 nm) while imposing a potential step inside the in-operando electrochemical chamber.

The stability of the sample under electrochemical cycling is guaranteed by the implementation of periodic control measurements. ***Supplementary Figure 4*** shows chronopotentiometry curves obtained before and after operando measurements. -1 μA current is imposed. No evidences of degradation are observed before and after the cycling steps.

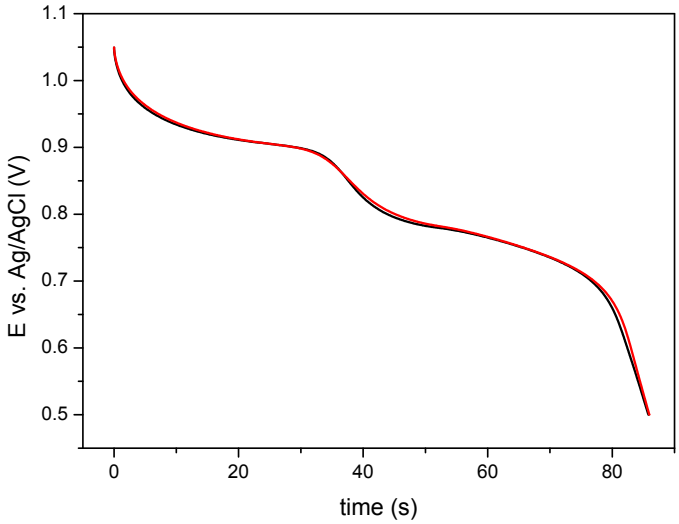

Supplementary Figure 4. Cronopotentiometry measurements taken before and after operando measurements.

4. Finite element model

The effect of nanoporosity on the litiation mechanism of LMO thin films was investigated by FEM analysis. COMSOL Multiphysics software was used with the Transport of diluted species module. The geometry consisted in a 2D axisymmetric Grain (see ***Supplementary Figure 5***). The grain dimension was varied between 60 and 100 nm. The thickness of the film was reported after the

ellipsometry measurements and corroborated by TEM images (not presented here). The nanoporosity was simulated by a lateral rectangle controlled by the parameters p an f (p = 2.5nm and f=0.8), that are defined in ***Supplementary Figure 5 a and b***. A constant Li concentration (cLi =1) was set on the upper and lateral surface of the grain (figure ***Supplementary Figure 5 b***). The solution was then computed in time dependent mode and the averaged Li concentration in the system calculated for different times. ***Supplementary Figure 5 d*** shows a characteristic evolution with time of the Li concentration in the system. Due to the pores, the upper part of the grain rapidly reaches the steady sate concentration, while the lower part presents a more classical 2D diffusion front.

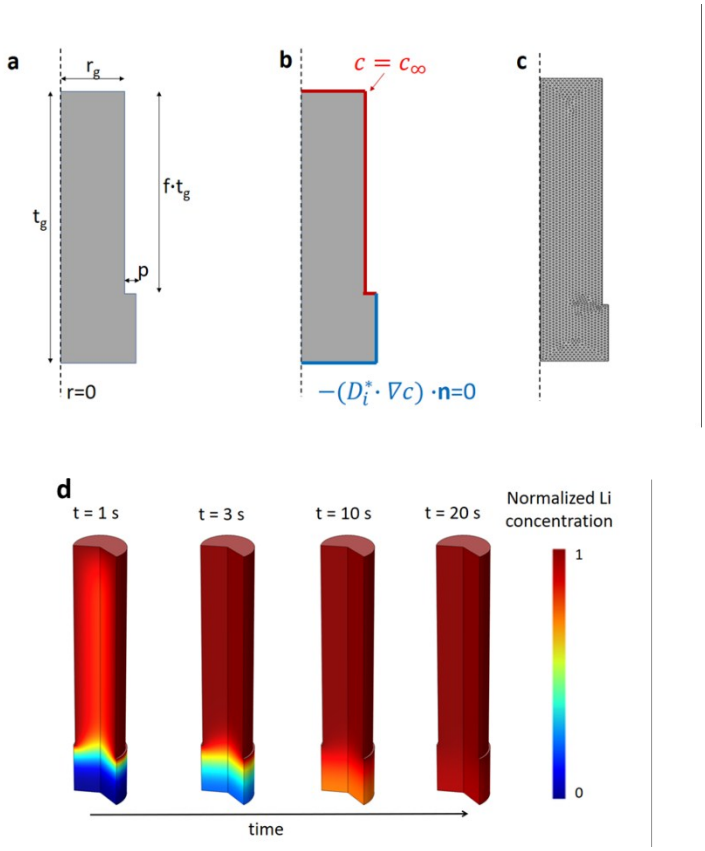

Supplementary Figure 5. Description of the geometry used for the FEM modelling (a, b). Meshing used (b). Evolution of the concentration of Li inside the columns (d).

Despite being a very simple approximation to a complex morphology (with diverse grain diameters, shapes, orientations etc.), it can be used to demonstrate the possible trends and to obtain an estimation of a Li+ diffusivity in the sample. For this proof of concept, different geometries and diffusivity values have been introduced in the model and compared with the experimental value until the reasonable matching of ***Supplementary Figure 6*** is obtained, which is obtained with a D_{eff} of $3.5 \cdot 10^{-12}$ $cm^2 s^{-1}$. Curves arising from models with different radius are also presented to give an idea of the sensitivity of the process. Varying the grain radius has an influence on the first part of the curve, while the second part is controlled by the diffusion

coefficient. Overall, the results show that a films with a particular microporosity may lead to the appearance of two different time constants in the concentration profiles.

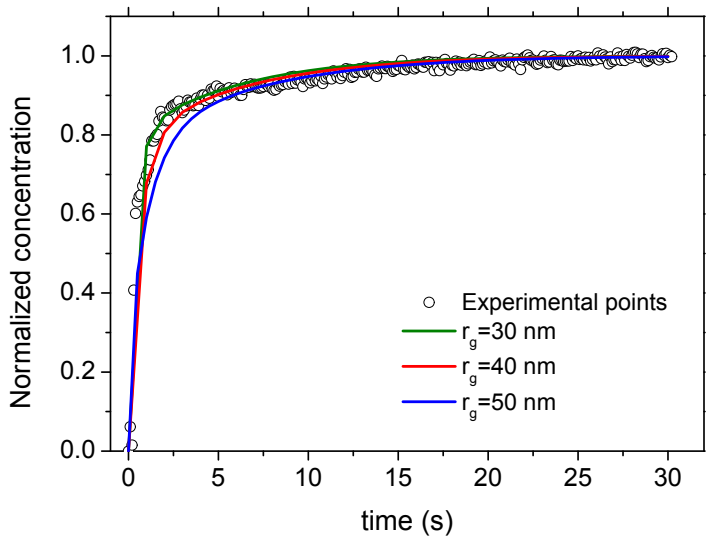

Supplementary Figure 6. Evolution of ε_i at 2.8 eV during this voltage step. The different lines represent the curves arising from the FEM model, with identical parameters but changing the grain radius.

[1] G. E. Jellison and F. A. Modine, "Parameterization of the optical functions of amorphous materials in the interband region," Appl. Phys. Lett., 69, 371-373 (1996).